



Nature inspired ZnO/ZnS nanobranch-like composites, decorated with Cu(OH)₂ clusters for enhanced visible-light photocatalytic hydrogen evolution

Puttaswamy Madhusudan, Yu Wang, Bananakere Nanjegowda Chandrashekhar, Weijun Wang, Jingwei Wang, Jun Miao, Run Shi, Yuxing Liang, Guojun Mi, Chun Cheng*

Department of Materials Science and Engineering, Southern University of Science and Technology, Shenzhen, PR China



ARTICLE INFO

Keywords:

ZnO/ZnS nanobranches
Cu(OH)₂ clusters
Hydrogen evolution
Visible-light irradiation
Photocatalysis

ABSTRACT

In this study, ZnO/ZnS hierarchical nanobranch like composite with Cu(OH)₂ clusters were designed via a simple facile hydrothermal process followed by precipitation reaction. Anchoring Cu(OH)₂ clusters on the ZnO/ZnS composite surface can shorten the charge migration distance, providing abundant active sites and extend the visible-light absorption. The effects of Cu(OH)₂ clusters loading on the photocatalytic application were investigated. The photocatalytic activities for hydrogen production were evaluated under visible-light ($\lambda > 400$ nm) irradiation. It was found that coupling suitable weight ratio of Cu(OH)₂ cluster over the ZnO/ZnS nanobranches will enhance the photocatalytic hydrogen evolution by 46.5 and 13.7 times higher than pure Zn₅(CO₃)₂(OH)₆ and ZnO/ZnS, nanobranches respectively and an apparent quantum efficiency of 11.5% at $\lambda = 420$ nm, and 14.7% under monochromatic LED light irradiation of 520 nm wavelength was achieved. This results show that construction of ZnO/ZnS nanobranches decorated with Cu(OH)₂ clusters can effectively improve the charge transfer and enhance the photocatalytic hydrogen production. The as-prepared ZnO/ZnS nanobranches decorated with Cu(OH)₂ clusters exhibits outstanding stability and recyclability. The mechanism for the enhanced hydrogen evolution is also discussed.

1. Introduction

The depletion of fossil fuels and increasing demand for energy has led researchers for the development of clean and renewable energy sources [1–3]. Hydrogen is believed to be one of the most promising alternatives for fossil fuels and source of sustainable green energy having potential ability to replace the conventional energy sources in future [4,5]. In this regard, solar light driven photocatalysis using semiconductors is one of the most promising green technologies for water splitting and generation of hydrogen fuel [6–8]. In recent years, a wide range of low-cost photocatalytic materials, including metal oxides, sulfides, carbon nitride, carbon based materials, and their composites have been shown to possess reasonable activity toward hydrogen evolution reaction [9–15]. Among these catalysts morphology controlled preparation of nanostructured ZnO/ZnS has drawn intense attention because of their useful optical and electrical properties and wide applications [16]. However, the utilization efficiency of ZnO/ZnS for water splitting has limited severely by the wide band gap of ZnO and rapid recombination of photogenerated electron and holes, and thereby leading weak light harvesting in visible-light region

[17,18]. Hence, much effort has been devoted to improve the utilization of solar light by extending the photoabsorption of ZnO/ZnS to the visible region, by doping metal, noble metal deposition, and narrow band-gap semiconductors coupling [19,20]. This kind of coupling with other co-catalysts can form effective interfacial contact and strong interaction between two components in the composite and lead to an enhanced photogenerated charge transfer and separation. Meanwhile, these dopants are not only costly for large-scale applications but also raise environmental contamination concerns because of the metal ion leaching. While, loading noble metal as a co-catalyst over ZnO/ZnS significantly enhances its hydrogen production performance for photocatalytic water splitting in the presence of sacrificial reagents. However, noble metals are rare, expensive and seriously restrict their large-scale application [21]. As a result, numerous efforts have been undertaken to replace noble-metals with low-cost earth abundant high-performance co-catalysts with reasonable activities for hydrogen evolution reaction [22,23].

Recently, copper containing species have shown excellent ability to enhance the photocatalytic hydrogen production. For instance, Wang and co-workers fabricated three-dimensional ZnO/CuO heterojunction

* Corresponding author.

E-mail address: chengc@sustc.edu.cn (C. Cheng).

branched nanowires grown on copper film or mesh substrates for photoelectrochemical solar hydrogen production in a neutral medium [24]. Lou et al. prepared lollipop-shaped uniform Cu@Cu₂O/ZnO heterojunction nanocomposites, which showed improved stability with remarkable enhanced photocatalytic performance of hydrogen generation [25]. Chang et al. prepared CuS-ZnS/Carbon nanotube films as immobilized photocatalysts for H₂ production. According to their results the deposition of CuS nanoparticles on the ZnS/Carbon nanotube films leads to higher photocatalytic activity, which can attribute to the effective electron-hole separation [26]. Li et al. prepared Cu₂O/TiO₂ composite photocatalyst with significantly improved performance of photocatalytic hydrogen evolution, which was attributed to the close contact between Cu₂O and TiO₂ improving the interfacial charge transfer and suppressing the charge recombination [27]. The work of Sreethawong et al. showed that Cu loaded TiO₂ exhibited two times higher enhanced hydrogen production than that of NiO loaded TiO₂ [28]. Xu and co-workers reported TiO₂ loaded with CuO exhibited higher hydrogen evolution than of Pt or Pd loaded TiO₂ [29]. Yu and co-workers have reported preparation of Cu(OH)₂ doped TiO₂ with significant performance of photocatalytic hydrogen evolution, which is attributed to the close contact between Cu(OH)₂ and TiO₂. They further found that Cu(OH)₂ content in the composite significantly influenced its hydrogen evolution activity [30]. Very recently Cao et al. incorporated Cu₂(OH)₂CO₃ clusters onto the surface of TiO₂ through a facile precipitation method. The obtained Cu₂(OH)₂CO₃/TiO₂ showed outstanding photocatalytic hydrogen production rate, which is comparable to that of Pt/TiO₂ photocatalyst [31]. Particularly, bare ZnS photocatalyst demonstrates high activity on H₂ evolution compared with ZnO because of the repaid generation of electron-hole pairs by photon energy and highly negative potential of excited electrons in the conduction band. However, the solo use of ZnO or ZnS catalysts is limited due to its relatively wide bandgap for the visible light condition. Therefore, in order to resolve this issue, doping ZnO/ZnS nanobranches with noble metal free Cu(OH)₂ electrocatalyst is required to accelerate the hydrogen evolution reaction on the semiconductor surface. Hence, it is desirable to develop the controllable synthesis of ZnO/ZnS heterostructures decorated with noble metal free co-catalyst.

In recent years biological materials with hierarchical morphologies have generated huge interest along with researchers. Among various biological morphologies, branch like structure with high surface areas and unique hierarchical structure favor light harvesting for photocatalysis. Moreover, from a biomimetic point of view, the fabrication process of branch like structured materials is more economical and environmental friendly. Hence, inspired from the nature we have explored a novel strategy that could mimic hierarchical branch like structure, which can capture light from nano to micron scales and enhance light-dependent photocatalytic reactions [32–37]. Herein, for the first time nanobranch-like ZnO/ZnS heterostructures have been successfully converted from hydrothermally prepared Zn₅(CO₃)₂(OH)₆ counterparts by calcinations followed by ZnS precipitation in Na₂S aqueous solution at room temperature. The resultant heterostructures show nanobranch-like morphology consisting of nanosheets with a size of 80–100 nm. Finally, Cu(OH)₂ clusters were deposited on the surface of as-prepared ZnO/ZnS heterostructure by a facile precipitation method. The photocatalytic H₂ evolution activity of ZnO/ZnS heterostructure decorated with Cu(OH)₂ clusters were evaluated under visible-light illumination. This work shows a possibility for the utilization of low cost Cu(OH)₂ as a substitute for noble metal Pt, to enhanced photocatalytic H₂ production activity under visible-light. Further, as-prepared samples were extensively characterized and investigated. The related mechanisms of interfacial charge transfer and enhancement of H₂-production activity by loading Cu(OH)₂ clusters were interpreted.

2. Experimental

2.1. Preparation of ZnO nanobranches

All the chemical reagents used in this study were of analytical grade and used as received. Distilled water was used in all experiments. Poly (ethylene glycol) (PEG) was purchased from Sinopharm Chemical Reagent Co. Ltd and its average molecular weight Mw was *ca.* 20,000 g mol⁻¹. Zinc nitrate (Zn(NO₃)₂·6H₂O) was purchased from Shanghai Macklin Biochemical Co., Ltd and urea (CO(NH₂)₂), was purchased from Sinopharm Chemical Reagent Co. Ltd. In a typical synthesis, 0.9 g of zinc nitrate was dissolved in 140 mL distilled water with magnetic stirring at room temperature for 30 min to obtain a clear solution. After that, 0.2 g of PEG 2 0,000 and 0.1 g urea was added to the solution, which was stirred for another 30 min, and then transferred to a 180 mL Teflon-lined stainless steel autoclave. The autoclave was maintained at 180 °C for 12 h for hydrothermal reaction. After the mixture was cooled naturally to room temperature, the yellowish white precipitates were centrifuged, washed with ethanol and distilled water five times, dried in an oven at 60 °C for 8 h to produce Zn₅(CO₃)₂(OH)₆ nanotrees. The corresponding product was denoted as ZC. Finally the as-prepared Zn₅(CO₃)₂(OH)₆ nanotrees were calcined in air at 500 °C for 2 h to produce ZnO nanobranches.

2.2. Synthesis of ZnO/ZnS nanobranches

The as-prepared 0.065 g of ZnO nanobranches were dispersed in 40 mL of deionized water containing 2.4 g of Na₂S·9H₂O and stirred for 24 h. Finally, ZnO/ZnS precipitated solution was centrifuged, washed with ethanol and distilled water several times, and dried in an vacuum oven at 60 °C for 8 h to produce ZnO/ZnS nanobranches. Finally, ZnS were prepared from as-prepared ZnO/ZnS architectures, a typical experiment is as follows: 0.0065 g of ZnO/ZnS nanobranches were added into 40 mL of deionized water containing 0.56 g of KOH. The mixture solution was kept at room temperature around 24 h and later washed with deionized water and absolute ethanol to obtain ZnS nanobranches.

2.3. Synthesis of Cu(OH)₂ decorated ZnO/ZnS nanobranches

Cu(OH)₂ decorated ZnO/ZnS nanobranch photocatalysts were prepared by a simple precipitation method. In a typical synthesis, 0.4 g of ZnO/ZnS was dispersed in 50 mL of 0.25 M NaOH aqueous solution, and then a certain volume of 0.0077 M Cu(NO₃)₂ aqueous solution was added drop wise under stirring. The mixed solutions were stirred for 6 h at room temperature. After that, the precipitates were washed with deionized water and ethanol five times. Finally, the washed precipitates were dried at 80 °C for 12 h. The nominal molar ratios of Cu(OH)₂ to (ZnO/ZnS + Cu(OH)₂), which hereafter is designated as R, where 0, 0.5, 2, 3, and 7 nominal mol% and the resulting samples were labeled as CZ0, CZ0.5, CZ2, CZ3, and CZ7, respectively. The actual chemical compositions of the prepared samples were measured by inductively coupled plasma atomic emission spectrometry (ICP-AES) using an Optima 4300 DV spectrometer (Perkin Elmer). For comparison, platinum was deposited onto CZ0 sample through photodeposition method. The typical preparation condition was as follows: 0.2 g of CZ0 sample was dispersed in a 50 mL of water and 1 wt % of H₂PtCl₆·6H₂O was dropped under stirring for 30 min. Then, the above suspension was stirred and irradiated by a 350 W Xe lamp. After irradiation for 30 min, the sample was washed with distilled water and collected by centrifugation and dried at 80 °C overnight. The obtained samples were denoted as Pt-CZ0.

2.4. Characterization

The powder X-ray diffraction (XRD) patterns of as-prepared samples were performed on an Rigaku D/max-2500 diffractometer with mono

Table 1Effect of copper content on the physicochemical properties and H₂ evolution rate for various samples.

Sample No	x	Cu (mol%) (ICP-AES)	S _{BET} (m ² g ⁻¹)	Pore volume (cm ³ g ⁻¹)	Pore size (nm)	Rate of H ₂ -production (μmol h ⁻¹ g ⁻¹)
ZC	0	0	14.1	0.047	13.42	29
CZ0	0	0	37.7	0.048	16.32	86
CZ0.5	0.5	0.37	28.3	0.096	10.17	777
CZ2	2	1.45	25.2	0.068	10.78	1350
CZ3	3	2.73	22.8	0.073	10.85	633
CZ7	7	6.24	18.9	0.065	10.78	325

chromatized Cu K α radiation (0.15418 nm) at a scan rate (20) of 0.05 s⁻¹. The accelerating voltage and applied current were 40 kV and 200 mA, respectively. Field emission scanning electron microscopy (FESEM, JSM-7500F, JEOL, Japan) images were recorded at an accelerating voltage of 10 kV and equipped with an energy-dispersive X-ray spectroscopy (EDS). The accurate concentrations of Cu²⁺ were detected using inductively coupled plasma atomic emission spectrometry (ICP-AES), (an Optima 4300 DV spectrometer, Perkin Elmer) and the values and mol%, respectively are shown in Table 1. The ZnO:ZnS mole percentage was detected using Vario EL cube elemental analyzer. The ZnO/ZnS composite sample (CZ2) was used in a tin boat assortment at 1000 °C in an oxygen atmosphere to determine the percentage composition of C, H, N and S elements. Transmission electron microscopy (TEM) and high-resolution transmission electron microscopy (HRTEM) analyses were conducted using Tecnai G2 20 U-Twin electron microscope operating at 200 kV. The Brunauer–Emmett–Teller (BET) specific surface area (S_{BET}) of the powders was analyzed by nitrogen adsorption in a Micromeritics ASAP 2020 nitrogen adsorption apparatus (USA). All the as-prepared samples were degassed at 180 °C prior to nitrogen adsorption measurements. The BET surface area was determined by a multipoint BET method using the adsorption data in the relative pressure (P/P_0) range of 0.05–0.3. A desorption isotherm was used to determine the pore size distribution via the Barret–Joyner–Halender (BJH) method, assuming a cylindrical pore model [38]. The nitrogen adsorption volume at the relative pressure (P/P_0) of 0.994 was used to determine the pore volume and average pore size. The X-ray photoelectron spectroscopy (XPS) measurement was performed in an ultra-high vacuum VG ESCALAB 210 electron spectrometer using Mg K α (1253.6 eV) radiation source (operating at 200 W) of a twin anode in the constant analyzer energy mode with a pass energy of 30 eV. All the binding energies were referenced to the adventitious C 1s line at 284.8 eV as the internal standard. UV-vis absorbance spectra of composite powders were obtained for the dry-pressed disk samples with a UV-vis spectrophotometer (PerkinElmer) using BaSO₄ as a standard.

2.5. Photocatalytic H₂ production

The photocatalytic hydrogen production experiments were performed in 100 mL Pyrex flask at ambient temperature and atmospheric pressure, and openings of the flask were sealed with silicone rubber septum. A 350 W Xe arc lamp (Changzhou SiyuEnvirontMater.Co., China) through a UV-cut-off filter ($\lambda > 400$ nm) positioned 5 cm in front of the photocatalytic reactor was used as visible-light source (22 cm far away from the photocatalytic reactor). The focused intensity on the flask measured by a visible-light radiometer (Model: FZ-A, China) was ca. 150 mWcm⁻² in the wavelength range of 420–1000 nm. In a typical photocatalytic experiments, 50 mg of catalyst was suspended in 80 mL mixed aqueous solution containing 0.35 M Na₂S and 0.25 M Na₂SO₃. Prior to irradiation, the suspensions were bubbled by nitrogen for 30 min to remove the dissolved oxygen and to ensure that the reaction system is under anaerobic condition. A continuous magnetic stirrer was applied at the bottom of the reactor in order to keep the photocatalyst particles in suspension state during the whole experiments. 0.4 mL of gas was intermediately sampled through the septum, and hydrogen concentration was analyzed by gas

chromatography (GC-14C, Shimadzu, Japan, TCD, nitrogen as a carrier gas and 5 Å molecular sieve column). All glassware was carefully rinsed with distilled water prior to use. The apparent quantum efficiency (QE) was also measured under the same photocatalytic reaction conditions except that the light source was different. Four LED (3 W, 420 or 520 nm, Shenzhen LAM-PLIC Science Co. Ltd., China), positioned 1 cm away from the reactor in four different direction, were used as light sources to trigger the photocatalytic reaction. The QE was calculated according to Eq. (1):

$$\text{QE}[\%] = \frac{\text{number of reacted electrons}}{\text{number of incident photons}} \times 100 \\ = \frac{\text{number of evolved H}_2\text{molecules} \times 2}{\text{number of incident photons}} \times 100 \quad (1)$$

2.6. Photoelectrochemical measurements

Photocurrents were measured by an electrochemical analyzer (CHI660C Instruments, CHI, China) in a standard three-electrode system using the prepared samples as the working electrodes with an active area of ca. 0.5 cm², a Pt wire as the counter electrode, and Ag/AgCl (saturates KCl) as a reference electrode. An LED (3 W, 420 nm, Shenzhen LAM-PLIC Science Co. Ltd., China), positioned 1 cm away from the reactor, were used as visible-light sources. The photoanode was kept at a 15 cm distance from the light source. The integrated visible-light intensity measured with a visible-light radiometer (FZ-A) was 80 mW/cm⁻². A 0.5 M Na₂SO₄ aqueous solution was used as the electrolyte. Working electrodes were prepared as follows: 0.05 g of photocatalyst (samples Zn₅(CO₃)₂(OH)₆, CZ0 and CZ2) were ground with 0.02 g of polyethylene glycol (PEG, molecular weight: 20,000) and 0.5 mL of ethanol to make a slurry. The slurry was then coated onto a 2 cm × 1.2 cm F-doped SnO₂ coated glass (FTO glass) electrode by the doctor blade technique. Next, these electrodes were dried in an oven and calcined at 500 °C for 30 min. All investigated electrodes have a similar film thickness of 10–11 μm.

3. Results and discussion

3.1. Phase structure and morphology

Fig. 1 shows the XRD patterns of as-prepared composite samples synthesized with different loading of Cu(OH)₂ clusters. The diffraction pattern of ZC sample is indexed with standard data of hexagonal phase of Zn₅(CO₃)₂(OH)₆ structure (JCPDS card no. 19-1458). After calcination at 500 °C, Zn₅(CO₃)₂(OH)₆ is converted into ZnO by release of H₂O and CO₂. When the ZnO/ZnS composites are treated in KOH solution, the characteristic peaks of ZnO disappears and only crystalline wurtzite structure of ZnS is observed (Fig. EIS1†) [39]. Apparently, after ZnS ion exchange reaction, it could be seen that only ZnO and ZnS phases were identified for Cu(OH)₂ decorated ZnO/ZnS photocatalysts (CZ0, CZ0.5, CZ2, CZ3, and CZ7). Furthermore, all the diffraction peaks can be indexed to the hexagonal wurtzite structure of ZnO (JCPDS card no. 79-0206) and cubic phase of ZnS (JCPDS card no. 05-0566). No other crystalline impurities were detected. The diffraction peaks of ZnO and ZnS are sharp and intense, indicating the highly crystalline nature of

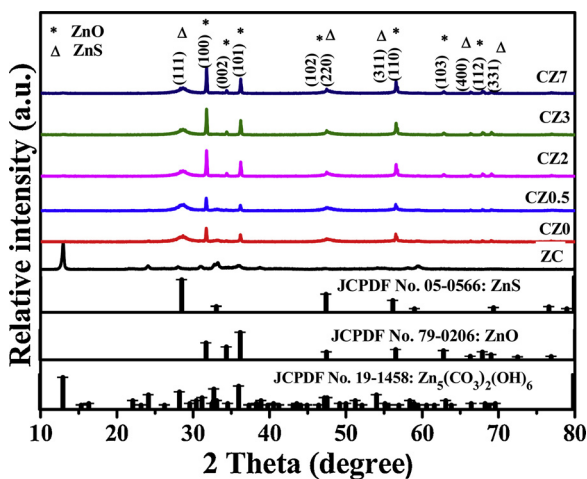


Fig. 1. XRD patterns of as-prepared ZC and CZ precursor samples along with standard diffraction patterns of $\text{Zn}_5(\text{CO}_3)_2(\text{OH})_6$, ZnO and ZnS.

ZnO/ZnS heterostructure composites [40]. In addition, it is noteworthy to mention that the intensity of (100) peak of ZnO is much higher than that of (101) plane, which suggests the anisotropic growth of ZnO sheets with exposed (100) planes [41]. It is noteworthy to comment that $\text{Cu}(\text{OH})_2$ phase could not be detected even when the Cu content is as high as 7% (CZ7). This phenomenon can be attributed to the fact that the $\text{Cu}(\text{OH})_2$ clusters loaded on the ZnO/ZnS surface have weak crystallization and could not be observed in the XRD. Nevertheless, the $\text{Cu}(\text{OH})_2$ clusters could be clearly observed in FESEM, TEM and XPS characterization results.

The FESEM, TEM and HRTEM measurements were performed to characterize the morphology and microstructure of the as-prepared samples. Fig. 2a, b shows the morphology of hydrothermally prepared $\text{Zn}_5(\text{CO}_3)_2(\text{OH})_6$ precursor before sintering, from which abundant branch-like nanostructure were observed. No other morphologies can be detected from the FESEM image, indicating a high yield of these nanostructures. The nanosheets were aligned from the stem to the surface to form hierarchical branches like structure. Fig. 2c shows typical FESEM image of hierarchical ZnO/ZnS nanocomposites (CZ0 sample), which are constructed by numerous two dimensional (2D) interlaced nanosheets (with thickness of ~100 nm), which resemble nanobranch like structure, clearly indicating the morphology and size of $\text{Zn}_5(\text{CO}_3)_2(\text{OH})_6$ precursor after sintering at 500 °C is preserved. Meanwhile, from the high resolution FESEM image of ZnO/ZnS nanobranches (Fig. 2d) it is very much clear that nanosheets are interconnected with each other with a thickness of 75–100 nm and an average 800–900 nm in width. Fig. 2e, f shows the FESEM images of $\text{Cu}(\text{OH})_2$ decorated ZnO/ZnS composite (CZ2 sample). It was clearly observed that the $\text{Cu}(\text{OH})_2$ clusters were uniformly deposited on the surface of the ZnO/ZnS nanosheets, and did not affect the branch-like ZnO/ZnS composite structures. As seen in Fig. 2f, the ZnO/ZnS nanobranches turned into rough surface after $\text{Cu}(\text{OH})_2$ cluster decoration. Moreover, the nanosheet building blocks of ZnO/ZnS composite acted as substrate to adhere $\text{Cu}(\text{OH})_2$ clusters and could provide more reactive sites, which were presumed to be favorable for photocatalytic activity. The CZ0 sample was further investigated by transmission electron microscopy (TEM). Abundant branches like nanostructures, packed closely with nanosheets are observed in Fig. 3a, which indicates the high yield of the morphology. As can be seen from the higher magnification TEM image the size and shape of the nanosheets are uniform (Fig. EIS2†). The TEM image of CZ2 composite sample shows branches-like structure, which are in agreement with FESEM results. The higher magnification TEM image of composite are illustrated in Fig. 3b which clearly indicates that the branches-like nanostructure which are 100–130 nm in thickness. Fig. 3d shows the corresponding

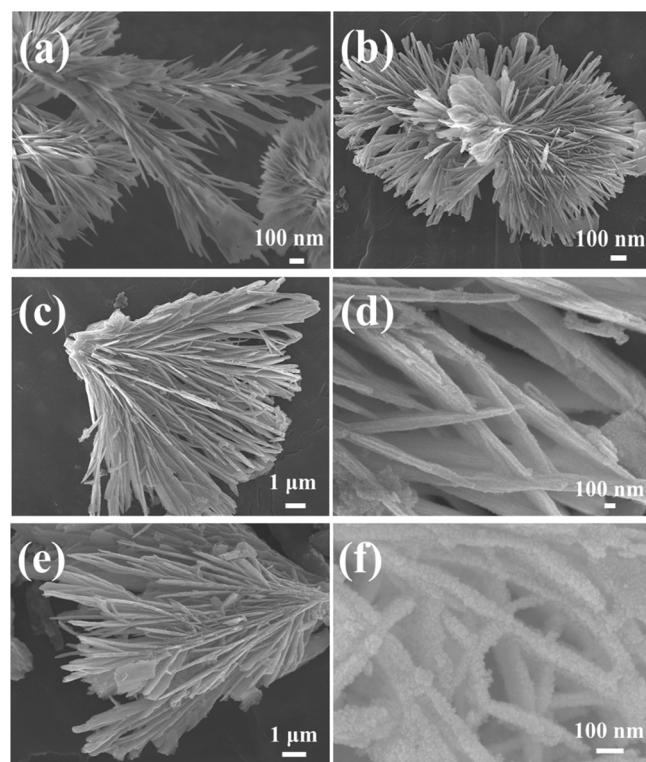


Fig. 2. FESEM images of as-prepared samples (a, b) $\text{Zn}_5(\text{CO}_3)_2(\text{OH})_6$ nanobranches, (c) ZnO/ZnS nanobranches heterostructure (CZ0), (d) high resolution of ZnO/ZnS nanobranches (CZ0), (e) $\text{Cu}(\text{OH})_2$ decorated ZnO/ZnS nanobranches (CZ2) and (f) high-resolution image of $\text{Cu}(\text{OH})_2$ cluster deposited ZnO/ZnS nanobranches (CZ2).

HRTEM image taken from the individual nanosheet. The fringe spacing of 0.28 nm agrees with the (100) lattice plane of hexagonal ZnO. Furthermore, the lattice spacing of ZnS is measured to be 0.31 nm, which corresponds to (111) crystal plane of ZnS [42,43]. Notably, it can be observed that some small $\text{Cu}(\text{OH})_2$ clusters with the size of ca. 2–5 nm are deposited on the surface of ZnO/ZnS nanobranches (as indicated in Fig. 2f). The deposited $\text{Cu}(\text{OH})_2$ nanoclusters should significantly increase the specific surface area of the nanospheres, which might benefit the photocatalytic activity of ZnO/ZnS composites. The lattice spacing of 0.25 nm can be indexed to (111) plane of $\text{Cu}(\text{OH})_2$ clusters. In order to evaluate the chemical uniformity of the particles in the CZ2 sample, the FESEM equipped with an energy dispersive spectrometry (EDS) characterization was employed. As shown in Fig. 4a the presence of Zn, O, S, C and Cu peaks which conform the phase purity of the as-prepared sample. The Al peak in the EDS spectra is originated from the sample grid. According to the CNHSO elemental analyzer results the weight percent composition of carbon, hydrogen, nitrogen and sulfur contents in CZ2 sample were as follows: N:C:H:S is 0.02:0.23:0.15:14.4 which is nearer to the experimental nominal molar percent. In order to further confirm the spatial distribution of each element in the as-prepared hierarchical nanobranch-like structures (CZ2 sample), electron mapping images of individual nanobranch were conducted and the corresponding results are shown in Fig. 4b. All the five major elements (Zn, O, S, C, and Cu) were uniformly distributed suggesting that the $\text{Cu}(\text{OH})_2$ clusters were deposited over the ZnO/ZnS nanobranches.

3.2. UV-vis diffuse reflectance spectra

The effect of $\text{Cu}(\text{OH})_2$ loading on the light absorption of the ZnO/ZnS composites are evaluated by UV-visible spectra (DRS). As shown in Fig. 5, the absorption edge of ZnO sample is strong in the UV region with the spectral wavelength between 200–400 nm. The steep

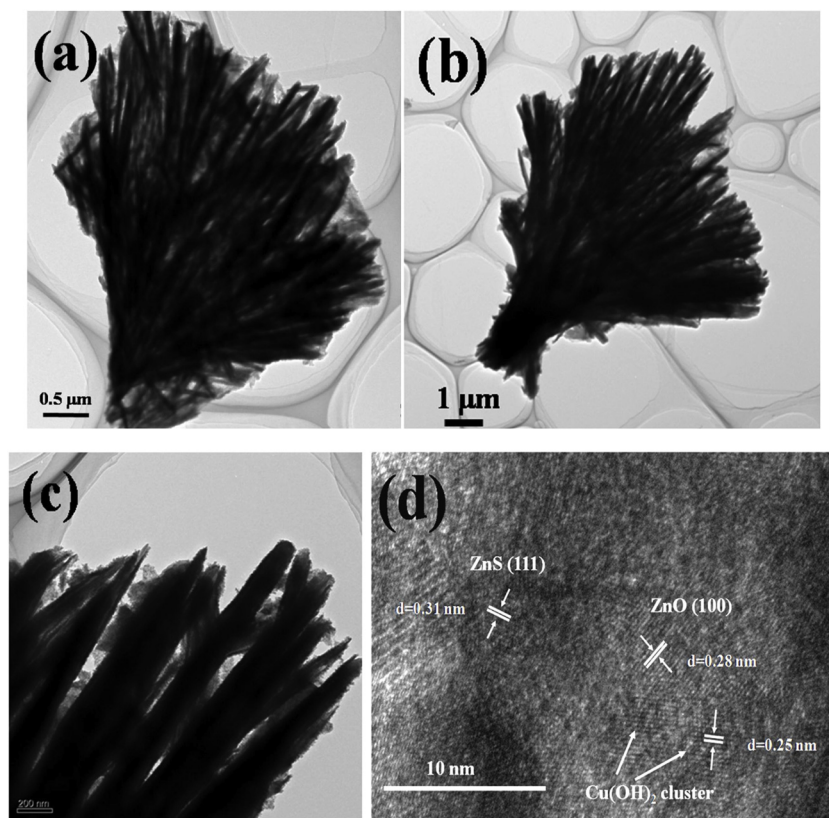


Fig. 3. TEM image of CZ0 (a), TEM and HRTEM image of as-prepared CZ2 sample (b-d).

absorption edge at 364 nm in ZnO corresponds to 3.4 eV, indicating UV-light intrinsic bandgap absorption due to the electronic transitions from the valence to the conduction band ($O_{2p} \rightarrow Zn_{3d}$) [44]. The onset of the absorption edge for ZnO/ZnS nanobranch-like heterostructure (CZ0) is at ca. 375 nm, which can be attributed to the intrinsic bandgap absorption of ZnS [45]. As expected, all Cu(OH)₂ decorated ZnO/ZnS heterostructure samples exhibit an increased absorption in the visible-light range in addition to the UV-light absorption band derived from ZnO/ZnS. This enhancement is ascribed to increasing in Cu(OH)₂ content, which has an obvious absorption in 300–800 nm range, implying that these samples have good visible-light photocatalytic activity. The absorption shoulder at 360–470 nm can be designated as the direct interfacial charge transfer (IFCT) and the absorption at 700–800 nm range can be assigned to the d-d transition of Cu(II) [46–48]. When the Cu(OH)₂ coupling level is low (< 2%), the color of the samples is light gray, and the shape of the diffuse reflectance spectra suggests that the coupling of Cu forms a new isolated energy level in the band structure of ZnO/ZnS heterostructures [49,50]. Furthermore, the visible-light absorption band shifts to a longer wavelength as the coupling amount increases and the corresponding color becomes dark gray.

3.3. XPS analysis

X-ray photoelectron spectroscopy analysis was employed to reveal the surface chemical composition and the detailed electronic states of different elements in CZ2 sample. The survey spectrum (Fig. 6a) indicates that the binding energy of 284.6, 531.5, 162.2, 1022 and 410.5 eV were attributed to C1s, O1s, S 2p, Zn 2p and Cu 2p respectively, indicating that Zn exist in the form of Zn²⁺ and S 2p peak at 162.2 eV implies that sulfur exists in the S²⁺ form. Fig. 6b shows the high-resolution XPS spectra of the C 1s region. There are three XPS peaks at around 284.7, 286.3 and 288.8 eV. The main peak at 284.7 eV is ascribed to the residual carbon and the adventitious hydrocarbon from the XPS instrument itself. The peak at 286.3 eV is associated with

Zn-O-C bonds and peak at 288.8 eV is related to adsorbed carbonate or carbon dioxide on the surface, which can induce the narrowing bandgap of ZnO/ZnS nanocomposites [51]. From the above results it is obvious that lattice C atom could be responsible for the red-shift in the absorption edge and the enhanced visible-light adsorption [52,53]. These results are in good agreement with the DRS analysis. Fig. 6c shows the high-resolution XPS spectra of Cu 2p region. The binding energies at ca. 932.5 and 952.4 eV correspond to Cu 2p_{3/2} and Cu 2p_{1/2} respectively. These binding energies indicate that the oxidation state of copper present on the surface of CZ2 sample is + 2. In addition, a very weak two shake-up lines (indicated by the arrows in Fig. 6c) located at 943.1 and 963.0 eV conforms to paramagnetic chemical state of Cu²⁺ [54]. The high resolution XPS spectra of Zn 2p, O 1s and S 2p are plotted in Fig. 6b–d, respectively. The high-resolution XPS spectrum of Zn 2p peaks appear doublet at ca. 1021.7 and 1044.8 eV, corresponding to Zn 2p_{3/2} and Zn 2p_{1/2} respectively, with a separation of 23.1 eV are assigned to Zn²⁺ state [55]. The XPS spectrum of O 1s region displays main peak at 531.8 eV which could be attributed to the Zn-O bonds in ZnO [56]. Meanwhile, the binding energy values of S 2p at ca. 161.6 and 162.5 eV are attributed to S 2p_{3/2} and S 2p_{1/2} transition, respectively. Furthermore, broadening of the S 2p peak indicates that presence of composite metal sulphides [57,58].

3.4. BET surface areas and pore size distributions

The effect of Cu(OH)₂ loading on the pore structure and BET surface areas of as-prepared samples are probed by the adsorption-desorption isotherms and the corresponding results of (ZC, CZ0 and CZ2) samples are shown in Fig. 7. It can be seen that, all the three samples shows type IV isotherms, with the hysteresis loop at high relative pressure, characteristic of mesoporous structure (2–50 nm) range [59]. Furthermore, at high P/P_0 range ($0.8 < P/P_0 < 1$), the shape of the hysteresis loop is of type H3, which are associated with narrow slit-shaped pores [60]. Further observations show that at medium P/P_0 range (< 0.4), the

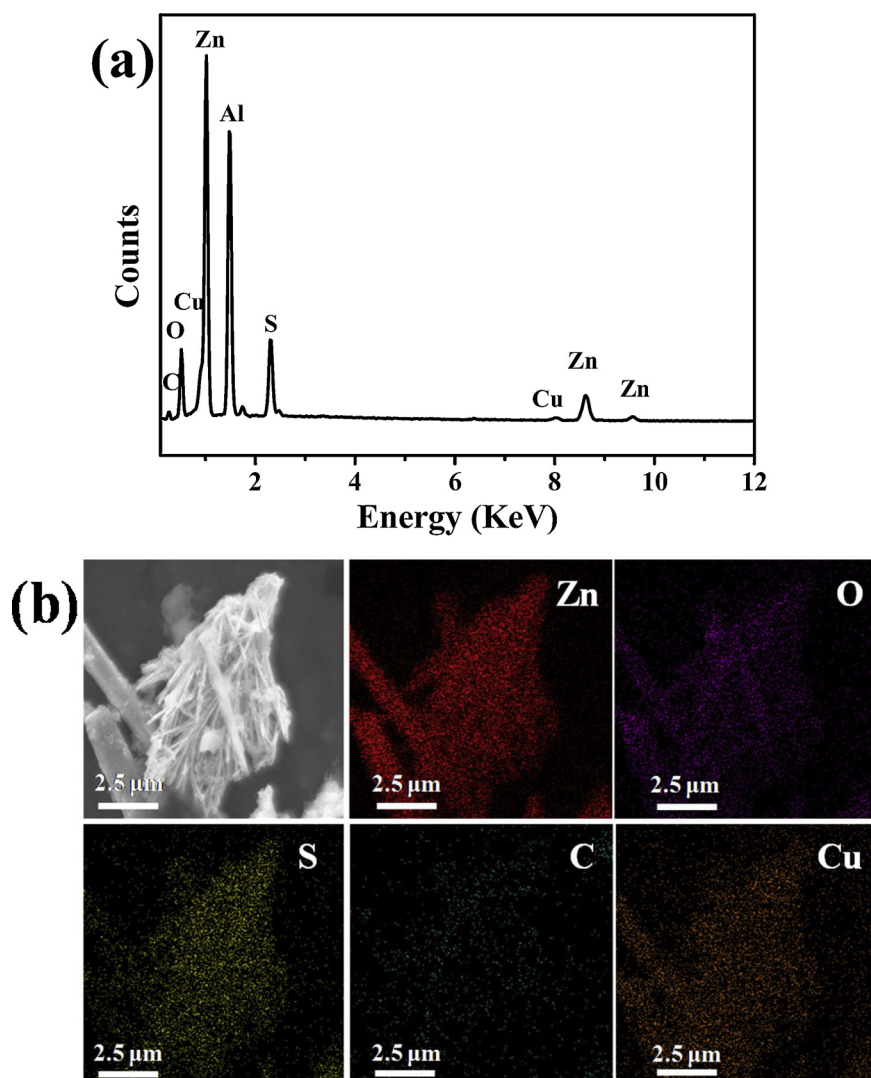


Fig. 4. (a) Energy dispersive X-ray spectroscopy (EDX) and (b) elemental mapping of CZ2 sample.

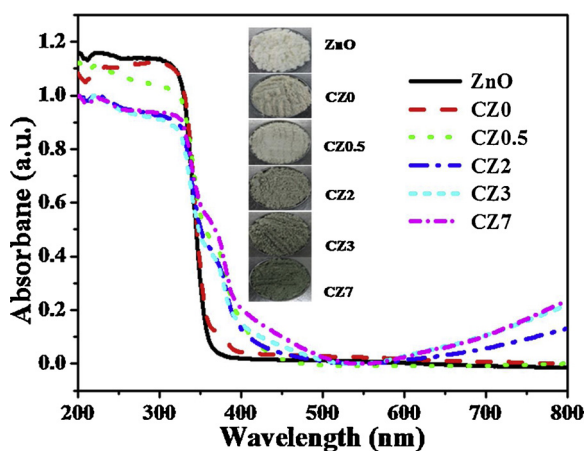


Fig. 5. UV-vis diffuse reflection spectra of as-prepared ZnO/ZnS nanobranches composites. The inset shows color variation of samples. (For interpretation of the references to color in text, the reader is referred to the web version of the article.).

isotherm of CZ2 sample shift upward compared to sample ZC and CZ0, suggesting higher surface area in CZ2 sample [61,62]. The pore-size distribution curves (inset of Fig. 7) calculated from the desorption

branch of the nitrogen isotherms by the BJH method show the wide range of 2–103 nm with a peak pore diameter of about 3.7 nm for sample CZ2, 3–120 nm with a peak pore diameter of about 49.7 nm for sample ZC and 45.3 nm for sample CZ0, further conforming the presence of mesopores and macropores [63–65]. The corresponding BET surface area values are listed in Table 1. With the increase of Cu(OH)₂ coupling the specific surface areas, pore volume and porosity is increased with comparison with ZC sample. The S_{BET} of the as-prepared samples slightly decreases as the content of Cu(OH)₂ cluster loading increased. The decrease in S_{BET} might be due to the Cu(OH)₂ loaded on the surface of ZnO/ZnS nanobranches have blocked up the pores.

3.5. Photocatalytic H₂-production activity

To investigate the photocatalytic properties of the as-prepared hierarchical ZnO/ZnS nanobranches, H₂ production were conducted under xenon arc lamp irradiation (with $\lambda > 400$ nm cutoff filter) using mixed aqueous solution containing 0.35 M Na₂S and 0.25 M Na₂SO₃ as a scavenger. Fig. 8a presents a comparison of the photocatalytic H₂ production activity of the as-prepared samples. The bare ZnO and ZnS catalyst shows very low H₂ production because of its unfavorable wide bandgap for the visible light condition. As can be seen from Fig. 8a, the Cu(OH)₂ loading has a substantial effect on the photocatalytic activity of ZnO/ZnS heterostructure. Without Cu(OH)₂ loading, the sample CZ0

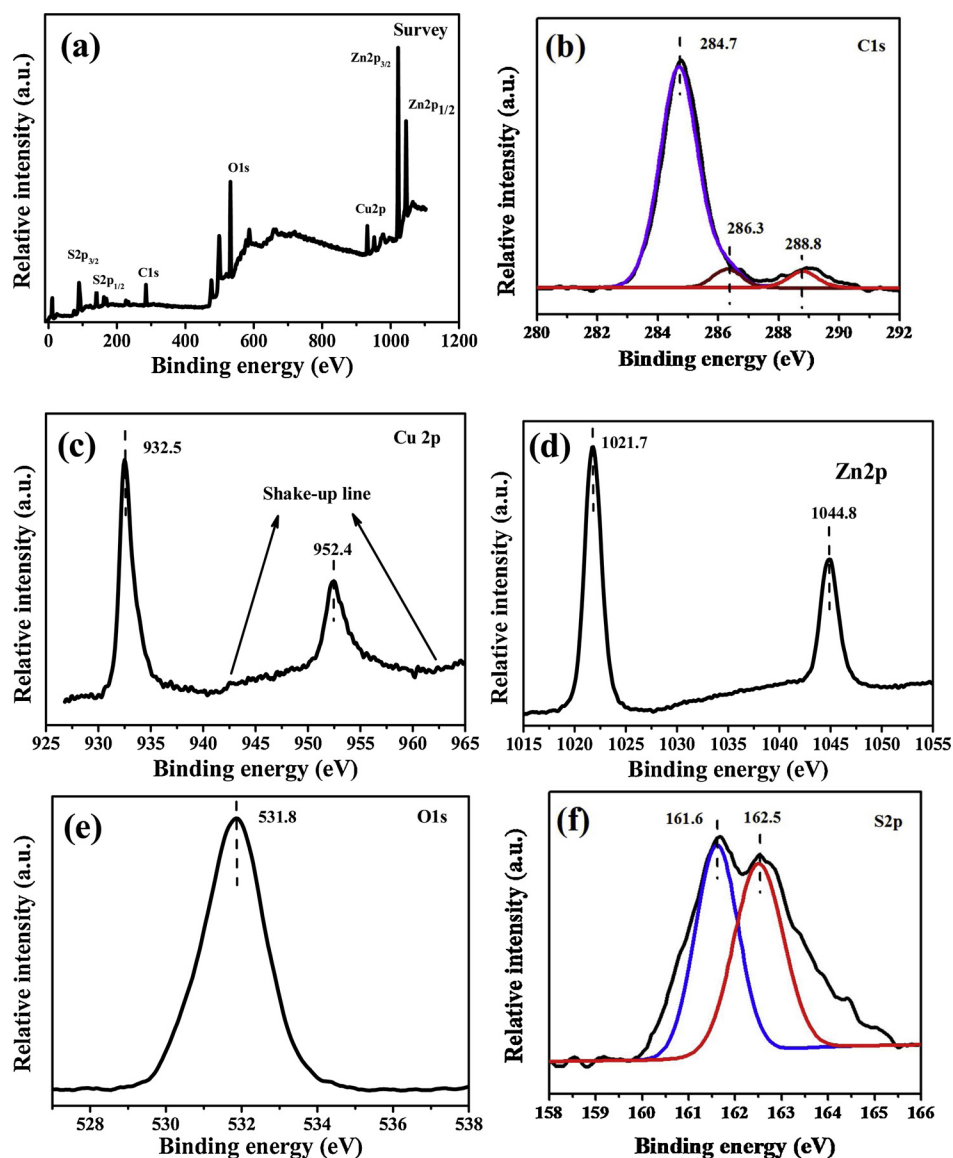


Fig. 6. High-resolution XPS spectrum (a), C 1s region (b), Cu 2p region (c), Zn 2p region (d), O 1s region (e), and S 2p region (f) of CZ2 sample.

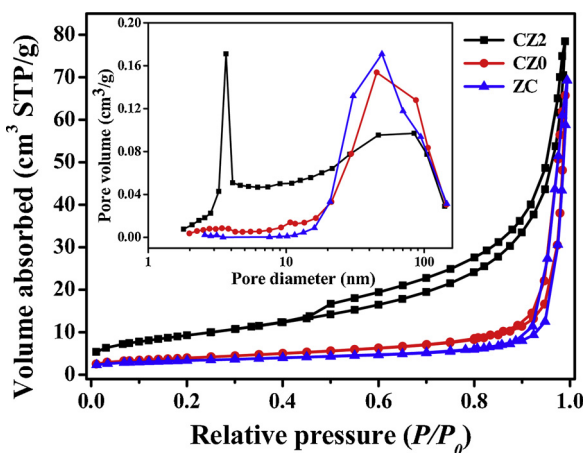


Fig. 7. Nitrogen adsorption–desorption isotherms and corresponding pore-size distribution curve (inset) of ZC, CZ0 and CZ2 sample.

shows a very low photocatalytic activity ($86 \mu\text{mol h}^{-1} \text{g}^{-1}$) because of the rapid recombination between CB electrons and VB holes in ZnO/ZnS heterostructure catalyst. After loading a small amount of Cu(OH)_2 clusters, the activity of the sample CZ0.5 is remarkably enhanced and increased by 9 times. The photocatalytic activity of the samples further increased with increasing Cu(OH)_2 content. The maximum H_2 -production rate, obtained for the CZ2 sample, is $1350 \mu\text{mol h}^{-1} \text{g}^{-1}$. To investigate the wavelength dependence photocatalytic H_2 evolution, the apparent quantum efficiencies (AQEs) of CZ2 sample for hydrogen evolution were examined over a visible-light range of 420 nm and 520 nm. The highest AQE value of 14.7% was achieved under 520 nm LED light illumination, while 11.5% was achieved at 420 nm. These results clearly illustrate that the hydrogen evolution reaction was indeed driven by the visible-light source. The photocatalytic H_2 -production for the CZ2 sample is 15.7 times higher than that of CZ0 sample and 46.5 times higher than that of ZC sample. When the Cu(OH)_2 loading is higher than 2 wt%, a decrease in H_2 -production is observed. Especially, at Cu(OH)_2 content is 7 wt%, the photocatalytic activity of the sample CZ5 drastically decreased to $325 \mu\text{mol h}^{-1} \text{g}^{-1}$ which is 4.1 times lower than CZ2 sample. This is perhaps due to the excessive deposition of Cu(OH)_2 clusters, might shield the ZnO/ZnS surface active sites. Further, increase in Cu(OH)_2 loading lead to a decrease of

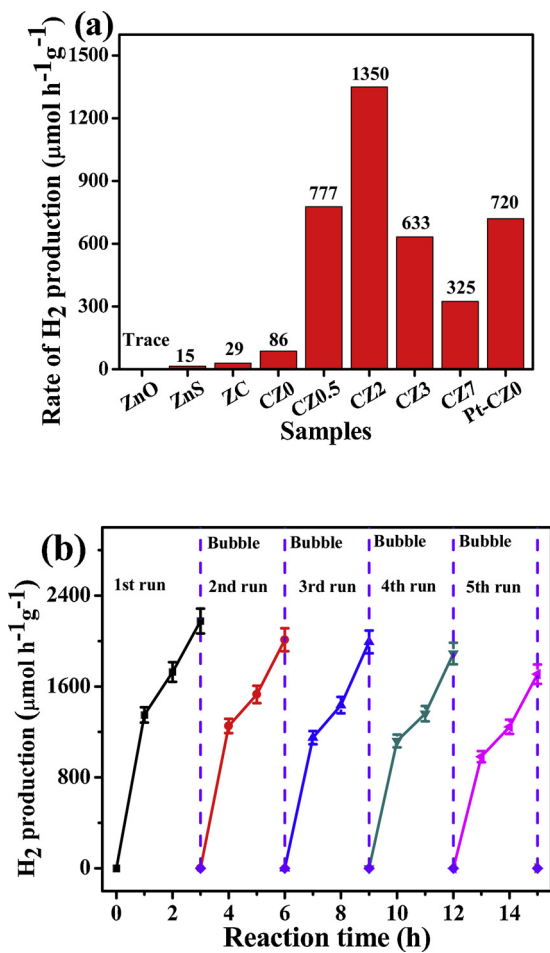


Fig. 8. (a) Photocatalytic H₂-production activities of as-prepared samples. (b) Time course of photocatalytic H₂ production over ZC2 sample from 0.35 M Na₂S and 0.25 M Na₂SO₃ aqueous solution under visible-light irradiation. The results are in good agreement within the error bar of around $\pm 5\%$.

irradiation passing through the reaction suspension solution. The present result reveals that suitable loading content of Cu(OH)₂ clusters is crucial for optimizing the photocatalytic behavior of semiconductor composites [30]. In addition, it is very interesting to know the activity of the ZnO/ZnS decorated with Cu(OH)₂ clusters is much higher than that of the platinum decorated ZnO/ZnS sample as shown in Fig. 8a. This reduction of H₂-evolution in Pt-CZO sample might be due to the metallic Pt co-catalyst can inhibit the fast recombination of oxygen and hydrogen into water, and thus reduce the over-potential during the formation of Schottky junction with the semiconductor photocatalysts, which encourage electron to participate in the catalytic process. Table 2 shows the photocatalytic H₂-evolution performance of various ZnO/ZnS based photocatalysts. It was found that the ZnO/ZnS decorated with Cu(OH)₂ clusters exhibits higher or comparable photocatalytic H₂ evolution activities compared with most of the previously reported ZnO/ZnS based photocatalysts. However, there are few ZnO/ZnS based composite materials showing higher H₂ evolution efficiency but these photocatalysts were modified either with noble metals such as PdS or with toxic CdS catalysts, which increases the cost of production or neither environment friendly for the large-scale usage. Therefore, the easily-prepared, non-noble metal Cu(OH)₂ clustering could still be of great interest for achieving high H₂ evolution efficiency. Furthermore, to the best of our understanding, this is the first report showing that an inexpensive novel metal-free Cu(OH)₂ loading can be used as an effective co-catalyst for photocatalytic water splitting over ZnO/ZnS hetero-nanostructures.

The stability of the CZ2 sample was further evaluated and the results are displayed in Fig. 8b. The H₂ production activity remains literally unchanged in the first and second runs, and slight decrease in successive runs, which is possible due to the continuous consumption of the sacrificial reagents (SO₃²⁻ and S²⁻). The above result indicates that CZ2 sample exhibits admirable stability and anti-photocorrosion capability during the photocatalytic reaction under visible-light. Besides, the comparison of the XRD patterns of CZ2 sample before and after the photocatalytic H₂ production is also demonstrated (Fig. EIS3†). Although the intensity of the diffraction peaks become weak, no significant difference in the XRD patterns can be observed, confirming that the as-prepared CZ2 photocatalyst are essentially stable and suitable for H₂-generation.

For effective photocatalytic H₂-production, the conduction band edge of a semiconductor photocatalyst should be more negative than the H⁺/H₂ potential. Therefore, it is of great importance to determine the band edges position of the as-prepared photocatalysts. Herein, the valence band (VB) edge positions and the conduction band (CB) edge positions of the ZnO, ZnS were estimated according to the following empirical formula [60]:

$$E_{VB} = \chi - E_e - 0.5E_g \quad (2)$$

where E_{VB} is the valence band edge potential, χ is the absolute electronegativity of the semiconductor, E_e is the energy of free electrons on the hydrogen scale (*ca.* 4.5 eV), E_{VB} is the VB edge potential and E_g is the band gap of the semiconductor. The conduction band position can be determined by $E_{CB} = E_{VB} - E_g$.

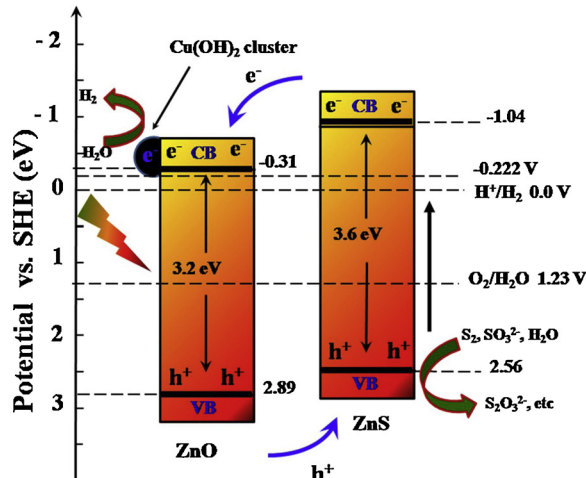
On the basis of the above results, the photocatalytic mechanism is tentatively proposed and shown in Fig. 9. The CB or ZnS is more negative potential than that of ZnO, whereas the VB of ZnO is more positive than that of ZnS [71,82]. Thus, it is speculated that the combination of ZnO with ZnS could be useful to accelerate the separation of electron-hole pairs for improving the photocatalytic H₂-production activity due to their matched energy band. Previously, such interfacial charge transfer phenomenon between two semiconducting materials is also reported by others [83,84]. Under visible-light irradiation, the photogenerated electrons from the CB of ZnS transfer to that of the ZnO, and holes on the VB of ZnO can transfer to that of the ZnS. Nevertheless, the CB edge of ZnS is more negative than the reduction potential of H⁺/H₂, the rate of H₂-production was negligible over bare ZnO/ZnS composites without Cu(OH)₂ loading. This can be assumed by considering the rapid recombination rate of CB electrons and VB holes and the presence of large H₂-production over-potential in ZnO/ZnS composites. The redox potential of the Cu(OH)₂/Cu is about -0.222 V (vs SHE, pH 0) [85], which, is a bit lower than the CB level of ZnO/ZnS (-0.31 V and -1.04 V, respectively), and promotes the electron transfer from the CB of ZnO to Cu(OH)₂ clusters and thus can release more free Cu²⁺ in aqueous solution. The visible light irradiation can reduce partial Cu²⁺ to Cu⁺ and Cu⁰ atoms. Leading to the effectively reduce protons to produce H₂ molecules [22,30].

To further understand the charge transfer and recombination behavior of the as-prepared photocatalytic materials, room temperature photoluminescence (PL) spectra under excitation wavelength of 325 nm were recorded and the corresponding results are illustrated in Fig. 10. It is noteworthy that the PL intensity for the CZ2 sample was greatly quenched compared to the other samples, indicating a low recombination of electron-hole pairs in the Cu(OH)₂ clustered ZnO/ZnS nanobranches sample greatly enhance of photocatalytic H₂ evolution activity.

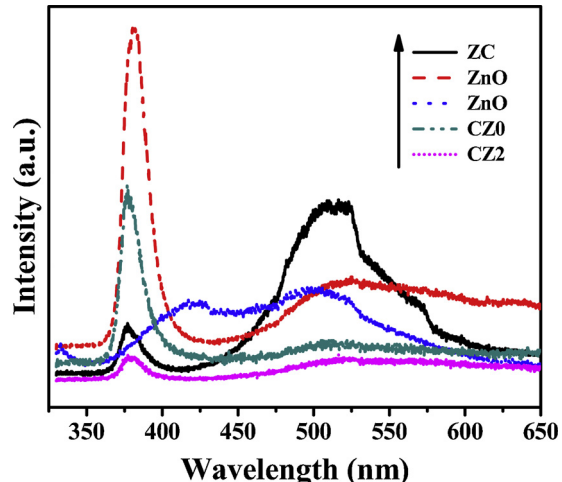
The photogenerated holes can be trapped by surface hydroxyl or water molecules to form high oxidative hydroxyl radical species. It has been reported that ·OH radicals could react with terephthalic acid (TA) to form 2-hydroxy-terephthalic acid (TAOH) that can emit fluorescence signal with a peak centered at 426 nm [86]. The qualitative formation rate of ·OH radical which are associated with the charge separation efficiency on the photocatalyst were measured by monitoring

Table 2Comparison of the photocatalytic H₂-production rates of water splitting over previously reported ZnO/ZnS based photocatalysts with those synthesized in this work.

Sl. No.	Photocatalyst	Reaction condition	Mass (mg)	Light source	Incidence light	Amount of H ₂ evolved	Reference No
1	ZnS/ZnO/ZnS nanosheets	0.35 M Na ₂ S and 0.25 M Na ₂ SO ₃	10	100 W Xe lamp	> 400 nm	79.8 μmol h ⁻¹ g ⁻¹	[66]
2	ZnS/ZnO nanocomposite	0.45 M Na ₂ S and 0.45 M Na ₂ SO ₃	10	300 W Xe lamp	> 400 nm	187 μmol g ⁻¹ h ⁻¹	[67]
3	ZnO-ZnS-CdS heterostructures	0.1 M Na ₂ S and 0.1 M Na ₂ SO ₃	200	500 W Xe lamp	≥ 420 nm	2790 μmol h ⁻¹ g ⁻¹	[68]
4	Ce doped ZnO/ZnS	0.1 M Na ₂ S and 0.04 M Na ₂ SO ₃ and 17.5 g NaCl in 100 mL water	100	500 W Hg-Xe arc lamp	–	1200 μmol h ⁻¹ g ⁻¹	[69]
5	ZnO/ZnS/CdS composite	5 g Na ₂ S and 5 g Na ₂ SO ₃ in 100 mL water	30	300 W Xe lamp	–	~ 11.37 mmol h ⁻¹ g ⁻¹	[70]
6	ZnS–ZnO hybridnanowires	0.25 M Na ₂ S and 0.35 M Na ₂ SO ₃	5	300 W Xe lamp	≥ 420 nm	22 μmol h ⁻¹ g ⁻¹	[71]
7	ZnO@ZnS/Ag@Ag ₂ S nanojunction	120 mL containing 25% by volume methanol	20	300 W Xe lamp	> 420 nm	140.3 μmol h ⁻¹ g ⁻¹	[72]
8	ZnO@ZnS–Bi ₂ S ₃ core–shell nanorod	230 mL of 5% glycerol	50	300 W Xe lamp	> 420 nm	310 μmol h ⁻¹ g ⁻¹	[73]
9	ZnO/ZnS Nanorod	50 mL H ₂ O containing 45 mL water and 5 mL glycerol	50	350 W Xe lamp	–	19.2 μmol h ⁻¹	[74]
10	ZnO/ZnS core–shell nanorods	10 mL 7% glycerol solution	300	500 W Xe lamp	–	388.4 μmol h ⁻¹ g ⁻¹	[75]
11	MOF-ZnO/ZnS Heteronanostructures	100 mL Na ₂ S (10.0 mmol) and Na ₂ SO ₃ (10.0 mmol)	50	300 W Xe lamp	> 420 nm	435 μmol h ⁻¹ g ⁻¹	[76]
12	ZnO-dotted porous ZnS microspheres	0.1 M Na ₂ S and 0.05 M Na ₂ SO ₃	40	300 W Xe lamp	≥ 200–400 nm	367 μmol g ⁻¹ h ⁻¹	[77]
13	ZnS–ZnO heterostructures	150 mL 60 mM sodium sulfide	100	150 W Xe lamp	≥ 420 nm	494.8 μmol g ⁻¹ h ⁻¹	[78]
14	Cu and Pt doped ZnO/ZnS core/shell nanotube	200 mL Na ₂ S (2.0 g) and Na ₂ SO ₃ (9.6 g)	200	350 W Xe lamp	> 420 nm	2.5 μmol h ⁻¹	[79]
15	ZnO/ZnS/graphene	Glycerol 40 vol%	50	300 W Hg lamp	–	1070 μmol h ⁻¹ g ⁻¹	[80]
16	ZnO/ZnS-PdS	5% glycerol	60	125 W He lamp	–	2141.9 μmol h ⁻¹ gcat ⁻¹	[81]
17	ZnO/ZnS-PdS	5% glycerol	60	500 W Xe lamp	–	238.1 μmol h ⁻¹ gcat ⁻¹	[81]
	ZnO/ZnS nanobranches decorated with Cu(OH) ₂ clusters	0.35 M Na ₂ S and 0.25 M Na ₂ SO ₃	50	350 W Xe lamp	> 400 nm	1350 μmol h ⁻¹ g ⁻¹	This work

**Fig. 9.** Proposed mechanism for the ZnO/ZnS photocatalytic reaction system.

fluorescence signal intensity of TAOH. The spectral changes of the CZ2 sample against light irradiation time and the comparison of the PL peak intensity of ZC, CZ0 and CZ2 samples are shown in Fig. 11a, b, respectively. The PL signals associated with the TAOH were observed with increasing irradiation time, indicating the generation of ·OH radicals upon visible-light irradiation (Fig. 11a). As illustrated in Fig. 11b, it is obvious the formation rate of ·OH for CZ2 is much larger than that of the other samples. This confirms that the loading of Cu(OH)₂ co-catalyst results in more effective charge separation and the photo-generated holes can produce more ·OH radicals toward stronger fluorescence signal. This implies that Cu(OH)₂ coupling over ZnO/ZnS has a lower recombination rate of electrons and holes under visible-light irradiation. This is ascribed to the fact that photoexcited electrons from the CB of ZnO and then migrate to Cu(OH)₂ co-catalysts, which prevent the direct recombination of charge carriers and play a major role as

**Fig. 10.** Study state photoluminescence spectra of as-prepared photocatalytic materials.reaction sites for H₂-production.

3.6. Transient photocurrent response analysis

Photoelectrochemical experiments were performed to examine the electronic interaction within the as-prepared samples (ZC, CZ0 and CZ2). It is clear from Fig. 12 that fast and uniform photocurrent responses are detected for each photocurrent on and off cycles of light irradiation and the photo-responsive phenomenon is entirely reversible. At 420 nm wavelength LED light irradiation, the photocurrent of the CZ2 sample is about 2.7 times as high as that of the CZ0 electrode and about 12 times as high as that of ZC electrode. Under visible-light irradiation, ZC sample shows almost small photocurrent response. The photocurrent enhancement of CZ2 electrode indicates an enhanced

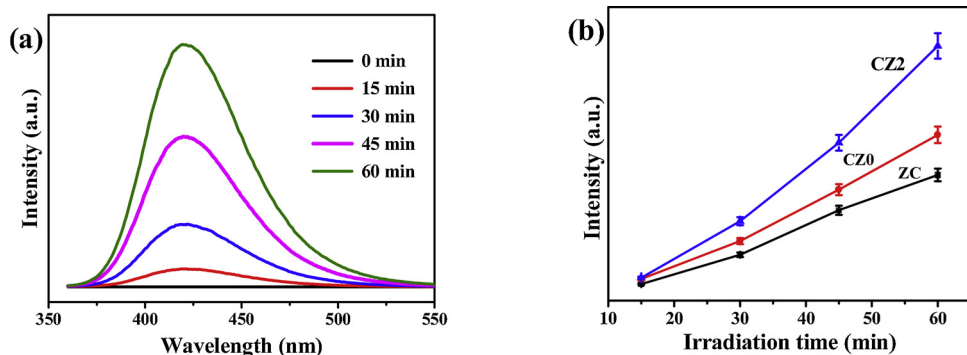


Fig. 11. (a) PL spectral changes observed during the illumination of the CZ2 sample in the presence of terephthalic acid in NaOH solution. (b) Comparison of PL peak intensity for the ZC, CZ0 and CZ2 samples against irradiation time with a error bar of around $\pm 5\%$.

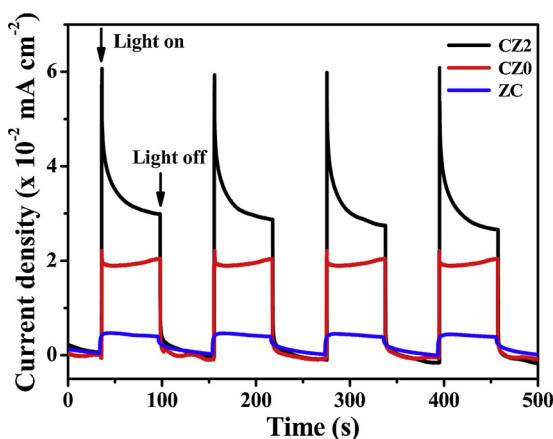


Fig. 12. Shows the transient photocurrent responses of ZC, CZ0 and CZ2 samples under-visible light irradiation (420 nm LED) in a 0.5 M aqueous solution of Na_2SO_4 .

separation of photogenerated electrons and holes, which could be attributed to the interaction of ZnO and ZnS with $\text{Cu}(\text{OH})_2$ clusters. Once more, this confirms why CZ2 composite sample has more excellent photocatalytic activity than that of CZ0 photocatalysts.

4. Conclusions

In summary, we developed novel ZnO/ZnS nanobranches decorated by $\text{Cu}(\text{OH})_2$ nanoclusters by a simple hydrothermal process followed by precipitation. The as-prepared ZnO/ZnS composites exhibited a nearly uniform size of nanobranches like morphology assembled by thin nanosheets. Further, these nanosheets are decorated by $\text{Cu}(\text{OH})_2$ nanoclusters. With 2 wt% loading of $\text{Cu}(\text{OH})_2$ nanoclusters on ZnO/ZnS nanobranches exhibited a higher H_2 production rate of $1350 \mu\text{mol h}^{-1} \text{ g}^{-1}$ under visible light illumination, which is 46.5 times higher than that for the $\text{Zn}_5(\text{CO}_3)_2(\text{OH})_2$ and 15.7 times higher than that for the ZnO/ZnS nanobranches samples. It is believed that the closer contact between $\text{Cu}(\text{OH})_2$ clusters and the ZnO/ZnS nanobranches can greatly suppress the charge recombination and provide a large number of active sites for photocatalytic reactions, thus significantly improving the photocatalytic hydrogen production activity. This study can also provide a new insight for the design and development of other ternary composite photocatalysts decorated by low cost co-catalysts as a substitute for noble metals for higher hydrogen production activity.

Conflicts of interest

There are no conflicts to declare.

Acknowledgements

The authors acknowledge the support from Guangdong Natural Science Funds for Distinguished Young Scholars (Grant 2015A030306044), National Natural Science Foundation of China (Grant 51776094, 51406075), Guangdong-Hong Kong joint innovation project (Grant 2016A050503012), the National Key Research and Development Project from the Ministry of Science and Technology (Grants 2016YFA0202400 and 2016YFA0202404), the Peacock Team Project funding from Shenzhen Science and Technology Innovation Committee (Grant No. KQTD2015033110182370), Training Program for Outstanding Young Teachers at Higher Education Institutions of Guangdong Province (Grant YQ2015151). Starting grants from Southern University of Science and Technology are also acknowledged.

Appendix A. Supplementary data

Supplementary data associated with this article can be found, in the online version, at <https://doi.org/10.1016/j.apcatb.2019.04.008>.

References

- [1] S. Chu, A. Majumdar, Opportunities and challenges for a sustainable energy future, *Nature* 488 (2012) 294–303.
- [2] A. Fujishima, K. Honda, Electrochemical photolysis of water at a semiconductor electrode, *Nature* 238 (1972) 37–38.
- [3] Z. Jun, L. Qi, J. Ran, J.G. Yu, S.Z. Qiao, Ternary $\text{NiS}/\text{Zn}_{1-x}\text{S}$ /reduced graphene oxide nanocomposites for enhanced solar photocatalytic H_2 -production activity, *Adv. Energy Mater.* 4 (2014) 1301925.
- [4] M.S. Dresselhaus, I.L. Thomas, Alternative energy technologies, *Nature* 414 (2001) 332–337.
- [5] R.D. Cortright, R.R. Davda, J.A. Dumesic, Hydrogen from catalytic reforming of biomass-derived hydrocarbons in liquid water, *Nature* 418 (2002) 964–967.
- [6] K. Maeda, K. Domen, Photocatalytic water splitting: recent progress and future challenges, *J. Phys. Chem. Lett.* 1 (2010) 2655–2661.
- [7] K. Maeda, Photocatalytic water splitting using semiconductor particles: History and recent developments, *J. Photochem. Photobiol. C-Photochem. Rev.* 12 (2011) 237–268.
- [8] X.W. Zhong, L.F. Zhang, J. Tang, J.W. Chai, J.C. Xu, L. Cao, M.Y. Yang, M. Yang, W.G. Kong, S. Wang, H. Cheng, Z.G. Lu, C. Cheng, B.M. Xu, H. Pan, Efficient coupling of hierarchical $\text{V}_2\text{O}_5@\text{Ni}_3\text{S}_2$ hybrid nanoarray for pseudocapacitors and hydrogen production, *J. Mater. Chem. A* 5 (2017) 17954–17962.
- [9] R. Van de Krol, Y.Q. Liang, J. Schoonman, Solar hydrogen production with nanostructured metal oxides, *J. Mater. Chem.* 18 (2008) 2311–2320.
- [10] A. Kudo, Y. Miseki, Heterogeneous photocatalyst materials for water splitting, *Chem. Soc. Rev.* 38 (2009) 253–278.
- [11] M.R. Hoffmann, S.T. Martin, W.Y. Choi, D.W. Bahnemann, Environmental applications of semiconductor photocatalysis, *Chem. Rev.* 95 (1995) 69–96.
- [12] S. Cao, J.G. Yu, $\text{g-C}_3\text{N}_4$ -based photocatalysts for hydrogen generation, *J. Phys. Chem. Lett.* 5 (2014) 2101–2107.
- [13] Q. Li, B.D. Guo, J.G. Yu, J.R. Ran, B.H. Zhang, H.J. Yab, J.R. Gong, Highly efficient visible-light-driven photocatalytic hydrogen production of CdS-cluster-decorated graphene nanosheets, *J. Am. Chem. Soc.* 133 (2011) 10878–10884.
- [14] L.F. Zhang, Y. Zhang, R. Shi, S.H. Bao, J.W. Wang, A. Amini, B.N. Chandrashekhar, C. Cheng, Improved Na-storage cycling of amorphous-carbon-sheathed Ni_3S_2 arrays and investigation by *in situ* TEM characterization, *Mater. Today Eng.* 5 (2017) 91–98.
- [15] A. Hezam, K. Namratha, Q.A. Drmosh, B.N. Chandrashekhar, K.K. Sudasivuni,

- Z.H. Yamani, C. Cheng, K. Byrappa, Heterogeneous growth mechanism of ZnO nanostructures and the effects of their morphology on optical and photocatalytic properties, *CystEngComm* 19 (2017) 3299–3312.
- [16] Y. Pina-Perez, O. Aguilar-Martinez, P. Acevedo-Pena, C.E. Santollana-Vargas, S. Oros-Ruiz, F. Galindo-Hernandez, R. Gomez, F. Tzompantzi, Novel ZnS-ZnO composite synthesized by the solvothermal method through the partial sulfidation of ZnO for H₂ production without sacrificial agent, *Appl. Catal. B-Environ.* 230 (2018) 125–134.
- [17] X.B. Chen, S.H. Shen, L.J. Guo, S.S. Mao, Semiconductor-based photocatalytic hydrogen generation, *Chem. Rev.* 110 (2010) 6503–6570.
- [18] C. Cheng, A. Amini, C. Zhu, Z. Xu, H.X. Song, N. Wang, Enhanced photocatalytic performance of TiO₂-ZnO hybrid nanostructures, *Sci. Rep.* 4 (2014) 4181.
- [19] M.H. Hsu, C.J. Chang, H.T. Weng, Efficient H₂ production using Ag₂S-coupled ZnO@ZnS core-shell nanorods decorated metal wire mesh as an immobilized hierarchical photocatalyst, *ACS Sustain. Chem. Eng.* 4 (2016) 1381–1391.
- [20] S.P. Lonkar, V.V. Pillai, S.M. Alhassan, Facile and scalable production of heterostructured ZnS-ZnO/Graphene nano-photocatalysts for environmental remediation, *Sci. Rep.* 8 (2018) 13401.
- [21] X.X. Zou, Y. Zhang, Noble metal-free hydrogen evolution catalysts for water splitting, *Chem. Soc. Rev.* 44 (2015) 5148–5180.
- [22] J.R. Ran, J. Zhang, J.G. Yu, M. Jaroniec, S.Z. Qiao, Earth-abundant cocatalysts for semiconductor based photocatalytic water splitting, *Chem. Soc. Rev.* 43 (2014) 7787–7812.
- [23] J.R. Ran, J. Zhang, J.G. Yu, S.Z. Qiao, Enhanced visible-light photocatalytic H₂ production by Zn_xCd_{1-x}S modified with earth-abundant nickel-based cocatalysts, *ChemSusChem* 7 (2014) 3426–3434.
- [24] A. Kargar, Y. Jing, S.J. Kim, C.T. Riley, X.Q. Pan, D.L. Wang, ZnO/CuO heterojunction branched nanowires for photoelectrochemical hydrogen generation, *ACS Nano* 7 (2013) 11112–11120.
- [25] Y.B. Lou, Y.K. Zhang, L. Cheng, J.X. Chen, Y.X. Zhao, A stable plasmonic Cu@Cu₂O/ZnO heterojunction for enhanced photocatalytic hydrogen generation, *ChemSusChem* 11 (2018) 1505–1511.
- [26] C.J. Chang, Y.H. Wei, W.S. Kuo, Free-standing CuS-ZnS decorated carbon nanotube films as immobilized photocatalysts for hydrogen production, *Int. J. Hydrogen Energy* (2018), <https://doi.org/10.1016/j.ijhydene.04.229>.
- [27] Y.P. Li, B.W. Wang, S.H. Liu, X.F. Duan, Z.Y. Hukey, Synthesis and characterization of Cu₂O/TiO₂ photocatalysts for H₂ evolution from aqueous solution with different scavengers, *App. Surf. Sci.* 324 (2015) 736–744.
- [28] T. Sreethawong, S. Yoshikawa, Comparative investigation on photocatalytic hydrogen evolution over Cu-, Pd-, and Au-loaded mesoporous TiO₂ photocatalysts, *Catal. Commun.* 6 (2005) 661–668.
- [29] S.P. Xu, D.D. Sun, Significant improvement of photocatalytic hydrogen generation rate over TiO₂ with deposited CuO, *Int. J. Hydrogen Energy* 34 (2009) 6096–6104.
- [30] J.G. Yu, J. Ran, Facile preparation and enhanced photocatalytic H₂-production activity of Cu(OH)₂ cluster modified TiO₂, *Energy Environ. Sci.* 4 (2011) 1364–1371.
- [31] Z.K. He, J.W. Fu, B. Cheng, J.G. Yu, S.W. Cao, Cu₂(OH)₂CO₃ clusters: novel noble-metal-free cocatalysts for efficient photocatalytic hydrogen production from water splitting, *Appl. Catal. B-Environ.* 205 (2017) 104–111.
- [32] P. Pathak, S. Gupta, K. Grosulak, H. Imahori, V. Subramanian, Nature-inspired tree-like TiO₂ architecture: a 3D platform for the assembly of CdS and reduced graphene oxide for photoelectrochemical processes, *J. Phys. Chem. C* 119 (2015) 7543–7553.
- [33] A. Ali, X.D. Li, J. Song, S. Yang, W. Zhang, Z.M. Zhang, R.X. Xia, L.X. Zhu, X.L. Xu, Nature-mimic ZnO nanoflowers architecture: chalcogenide quantum dots coupling with ZnO/ZnTiO₃ nanostructures for efficient photoelectrochemical water splitting, *J. Phys. Chem. C* 121 (2017) 21096–21104.
- [34] X.F. Zheng, G.F. Shen, C. Wang, Y. Li, D. Dunphy, T. Hasan, C.J. Brinker, B.L. Su, Bio-inspired murray materials for mass transfer and activity, *Nat. Commun.* 8 (2017) 11492.
- [35] Y. Zhang, L.L. Wu, X.Y. Zhao, Y.N. Zhao, H.Q. Tan, X. Zhao, Y.Y. Ma, Z. Zhao, S.Y. Song, Y.H. Wang, Y.G. Li, Leaf-mosaic-inspired vine-like graphitic carbon nitride showing high light absorption and efficient photocatalytic hydrogen evolution, *Adv. Energy Mater.* 8 (2018) 1801–2139.
- [36] X. Chen, W.Y. Lu, T.F. Xu, N. Li, D.D. Qin, Z.X. Zhu, G.Q. Wang, W.X. Chen, A bio-inspired strategy to enhance the photocatalytic performance of g-C₃N₄ under solar irradiation by axial coordination with hemin, *Appl. Catal. B-Environ.* 201 (2017) 518–526.
- [37] G.G. Liu, T. Wang, H.B. Zhang, X.G. Meng, D. Hao, K. Chang, P. Li, T. Kako, J.H. Ye, Nature-inspired environmental “Phosphorylation” boosts photocatalytic H₂ production over carbon nitride nanosheets under visible-light irradiation, *Angew. Chem. Int. Ed.* 54 (2015) 13561–13565.
- [38] K.S.W. Sing, D.H. Everett, R.A.W. Haul, L. Moscou, R.A. Pierotti, J. Rouquerol, T. Siemieniewska, Reporting physisorption data for gas/solid systems with special reference to the determination of surface area and porosity, *Pure Appl. Chem.* 57 (1985) 603–619.
- [39] Z.H. Jing, J.H. Zhan, Fabrication and gas-sensing properties of porous ZnO nanoplates, *Adv. Mater.* 20 (2008) 4547–4551.
- [40] X. Huang, M. Wang, M.G. Willinger, L.D. Shao, D.S. Su, X.M. Meng, Assembly of three-dimensional hetero-epitaxial ZnO/ZnS core/shell nanorod and single crystalline Hollow ZnS nanotube arrays, *ACS Nano* 6 (2012) 7333–7339.
- [41] L. Feng, C. Cheng, M. Lei, N. Wang, M.M.T. Loy, Spatially resolved photoluminescence study of single ZnO tetrapods, *Nanotechnology* 19 (2008) 405702.
- [42] J.G. Yu, J. Zhang, S.W. Liu, Ion-exchange synthesis and enhanced visible-light photoactivity of CuS/ZnS nanocomposite hollow spheres, *J. Phys. Chem. C* 114 (2010) 13642–13649.
- [43] S. Yue, B.W. Wei, X. Guo, S.X. Yang, L. Wang, J. He, Novel Ag₂S/ZnS/carbon nanofiber ternary nanocomposite for highly efficient photocatalytic hydrogen production, *Catal. Commun.* 76 (2016) 37–41.
- [44] J.G. Yu, X.X. Yu, Hydrothermal synthesis and photocatalytic activity of zinc oxide hollow spheres, *Environ. Sci. Technol.* 42 (2008) 4902–4907.
- [45] J. Zhang, J.G. Yu, Y.M. Zhang, Q. Li, J.R. Gong, Visible light photocatalytic H₂-production activity of CuS/ZnS porous nanosheets based on photoinduced interfacial charge transfer, *Nano Lett.* 11 (2011) 4774–4779.
- [46] X.Q. Qiu, M. Miyachi, H.G. Yu, H. Irie, K. Hashimoto, Visible-light-driven Cu (II)-(Sr_{1-y}Nay)(Ti_{1-x}Mox)O₃ photocatalysts based on conduction band control and surface ion modification, *J. Am. Chem. Soc.* 132 (2010) 15259–15267.
- [47] H.G. Yu, H. Irie, K. Hashimoto, Conduction band energy level control of titanium dioxide: toward an efficient visible-light-sensitive photocatalyst, *J. Am. Chem. Soc.* 132 (2010) 6898–6899.
- [48] H. Irie, K. Kamiya, T. Shibamura, S. Miura, D.A. Tryk, T. Yakoyama, K. Hashimoto, Visible light-sensitive Cu(II)-grafted TiO₂ photocatalysts: activities and X-ray absorption fine structure analyses, *J. Phys. Chem. C* 113 (2009) 10761–10766.
- [49] A. Kudo, M. Sekizawa, Photocatalytic H₂ evolution under visible light irradiation on Ni-doped ZnS photocatalyst, *Chem. Commun.* (2000) 1371–1372.
- [50] Z.H. Zhou, F.S. Han, L.J. Guo, O.V. Prezhdo, Understanding divergent behaviors in the photocatalytic hydrogen evolution reaction on CdS and ZnS: a DFT based study, *Phys. Chem. Chem. Phys.* 18 (2016) 16862–16869.
- [51] L. Ramqvist, K. Hamrin, G. Johansson, A. Fahlman, C. Nordling, Charge transfer in transition metal carbides and related compounds studied by ESCA, *J. Phys. Chem. Solids* 30 (1969) 1835–1847.
- [52] H. Pan, J.B. Yi, L. Shen, R.Q. Wu, J.H. Yang, J.Y. Lin, Y.P. Feng, J. Ding, L.H. Van, J.H. Yin, Room-temperature ferromagnetism in carbon-doped ZnO, *Phys. Rev. Lett.* 99 (2007) 127201.
- [53] S.W. Liu, C. Li, J.G. Yu, Q.J. Xiang, Improved visible-light photocatalytic activity of porous carbon self-doped ZnO nanosheet-assembled flowers, *CrystEngComm* 13 (2011) 2533–2541.
- [54] L.M. Liu, W. Yang, S. Gao, J.K. Shang, Synthesis of Cu₂O nanospheres decorated with TiO₂ nanoislands, their enhanced photoactivity and stability under visible light illumination, and their post-illumination catalytic memory, *ACS Appl. Mater. Interfaces* 6 (2014) 5629–5639.
- [55] X.W. Wang, B. Yuan, Z.H. Xie, D.X. Wang, R.B. Zhang, ZnS-CdS/Graphene oxide heterostructures prepared by a light irradiation-assisted method for effective photocatalytic hydrogen generation, *J. Colloid Interface Sci.* 446 (2015) 150–154.
- [56] S.S. Patil, M.A. Johar, M.A. Hassan, D.R. Patil, S.W. Ryu, Anchoring MWCNTs to 3D honeycomb ZnO/GaN heterostructures to enhancing photoelectrochemical water oxidation, *Appl. Catal. B-Environ.* 237 (2018) 791–801.
- [57] J. Shan, P. Pukkinen, U. Vainio, J. Maijala, J. Merta, H. Jiang, R. Serimaa, E. Kauppinen, H. Tenhu, Synthesis and characterization of copper sulphide nanocrystallites with low sintering temperatures, *J. Mater. Chem.* 18 (2008) 3200–3208.
- [58] J. Wang, Y.F. Lim, G.W. Ho, Carbon-ensemble-manipulated ZnS heterostructures for enhanced photocatalytic H₂ evolution, *Nanoscale* 6 (2014) 9673–9680.
- [59] J.W. Fu, B.C. Zhu, W. You, M. Jaroniec, J.G. Yu, A flexible bio-inspired H₂-production photocatalyst, *Appl. Catal. B-Environ.* 220 (2018) 148–160.
- [60] P. Madhusudan, J.R. Ran, J. Zhang, J.G. Yu, G. Liu, Novel urea assisted hydrothermal synthesis of hierarchical BiVO₄/Bi₂O₃O₂ nanocomposites with enhanced visible-light photocatalytic activity, *Appl. Catal. B-Environ.* 110 (2011) 286–295.
- [61] D. Xu, B. Cheng, S. Cao, J.G. Yu, Enhanced photocatalytic activity and stability of Z-scheme Ag₂CrO₄-GO composite photocatalysts for organic pollutant degradation, *Appl. Catal. B-Environ.* 164 (2015) 380–388.
- [62] Z.H. Zhang, L. Huang, J.J. Zhang, F.J. Wang, Y. Xie, X.T. Shang, Y. Gu, H. Zhao, X. Wang, In situ constructing interfacial contact MoS₂/ZnIn₂S₄ heterostructure for enhancing solar photocatalytic hydrogen evolution, *Appl. Catal. B-Environ.* 233 (2018) 112–119.
- [63] T. Soboleva, X. Zhao, K. Malek, Z. Xie, T. Navessin, S. Holdcroft, On the micro-, meso-, and macroporous structures of polymer electrolyte membrane fuel cell catalyst layers, *ACS Appl. Mater. Interfaces* 2 (2010) 375–384.
- [64] Q.L. Xu, B. Cheng, J.G. Yu, G. Liu, Making co-condensed amorphous carbon/g-C₃N₄ composites with improved visible-light photocatalytic H₂-production performance using Pt as cocatalyst, *Carbon* 118 (2017) 241–249.
- [65] H.X. Sang, X.T. Wang, C.C. Fan, F. Wang, Enhanced photocatalytic H₂ production from glycerol solution over ZnO/ZnS core/shell nanorods prepared by a low temperature route, *J. Hydrogen Energy* 37 (2012) 1348–1355.
- [66] X. Zhang, Y.Z. Zhou, D.Y. Xu, X.H. Liu, R. Zhang, H. Liu, C.K. Dong, J. Yang, S.A. Kulinich, W. Du, ZnO nanosheets with atomically thin ZnS overlayers for photocatalytic water splitting, *J. Mater. Chem. A* 6 (2018) 9057–9063.
- [67] H. Zhao, Y.M. Dong, P.P. Jiang, X.M. Xu, R.X. Wu, Y.M. Chen, Facile preparation of a ZnS/ZnO nanocomposite for robust sunlight photocatalytic H₂ evolution from water, *RSC Adv.* 5 (2015) 6494–6500.
- [68] X.W. Wang, G. Liu, Z.G. Chen, F. Li, Highly efficient H₂ evolution over ZnO-ZnS-CdS heterostructures from an aqueous solution containing SO₃²⁻ and S²⁻ ions, *J. Mater. Res.* 25 (2010) 39–44.
- [69] C.J. Chang, K.L. Huang, J.K. Chen, K.W. Chu, M.H. Hsu, Improved photocatalytic hydrogen production of ZnO/ZnS based photocatalysts by Ce doping, *J. Taiwan Inst. Chem. Eng.* 55 (2015) 82–89.
- [70] R.L. Zhang, J.W. Xie, C. Wang, J. Liu, X.F. Zheng, Y. Li, X.Y. Yang, H.E. Wang, R.L. Su, Macroporous ZnO/ZnS/CdS composite spheres as efficient and stable photocatalysts for solar-driven hydrogen generation, *J. Mater. Sci.* 52 (2017) 11124–11134.
- [71] Z. Wang, S.W. Cao, S.C.J. Loo, C. Xue, Nanoparticle heterojunctions in ZnS-ZnO hybrid nanowires for visible-light-driven photocatalytic hydrogen generation, *CrystEngComm* 15 (2013) 5688–5693.
- [72] Y.P. Su, Z.C. Zhao, S. Li, F. Liu, Z.T. Zhang, Rational design of a novel quaternary

- ZnO@ZnS/Ag@Ag₂S nanojunction system for enhanced photocatalytic H₂ production, Inorg. Chem. Front. 5 (2018) 3074–3081.
- [73] W. Xitao, L. Rong, W. Kang, Synthesis of ZnO@ZnS-Bi₂S₃ core-shell nanorod grown on reduced graphene oxide sheets and its enhanced photocatalytic performance, J. Mater. Chem. A 2 (2014) 8304–8313.
- [74] D. Bao, P. Gao, X. Zhu, S. Sun, Y. Wang, X. Li, Y. Chen, H. Zhou, Y. Wang, P.P. Yang, ZnO/ZnS heterostructured nanorod arrays and their efficient photocatalytic hydrogen evolution, Chem. Eur. J. 21 (2015) 12728–12734.
- [75] H.X. Sang, X.T. Wang, C.C. Fan, F. Wang, Enhanced photocatalytic H₂ production from glycerol solution over ZnO/ZnS core/shell nanorods prepared by a low temperature route, Int. J. Hydrogen Energy 37 (2012) 1348–1355.
- [76] X.X. Zhao, J.R. Feng, J.W. Liu, J. Lu, W. Shi, G.M. Yang, G.C. Wang, P.Y. Feng, P. Cheng, Metal-organic framework-derived ZnO/ZnS heteronanostructures for efficient visible-light-driven photocatalytic hydrogen production, Adv. Sci. 5 (2018) 1700–2590.
- [77] A.P. Wu, L.Q. Jing, J.Q. Wang, Y. Qu, Y. Xie, B.J. Jiang, C. Tian, H.G. Fu, ZnO-dotted porous ZnS cluster microspheres for high efficient, Pt-free photocatalytic hydrogen evolution, Sci. Rep. 5 (2015) 8858.
- [78] E. Hong, J.H. Kim, Oxide content optimized ZnS-ZnO heterostructures via facile thermal treatment process for enhanced photocatalytic hydrogen production, Int. J. Hydrogen Energy 39 (2014) 9985–9993.
- [79] D.W. Jing, R. Li, M.C. Liu, L.J. Guo, Copper-doped ZnO/ZnS core/shell nanotube as a novel photocatalyst system for photocatalytic hydrogen production under visible light, Int. J. Nanotechnol. 8 (6/7) (2011) 446–457.
- [80] C.J. Chang, Y.G. Lin, H.T. Weng, Y.H. Wei, Photocatalytic hydrogen production from glycerol solution at room temperature by ZnO-ZnS/graphene photocatalysts, Appl. Surf. Sci. 451 (2018) 198–206.
- [81] S. Liu, X. Wang, K. Wang, R. Lv, Y. Xu, ZnO/ZnS-PdS core-shell nanorods: synthesis, characterization and application for photocatalytic hydrogen production from a glycerol/water solution, Appl. Surf. Sci. 283 (2013) 732–739.
- [82] C. Cheng, Y.T. Shi, C. Zhu, W. Li, L. Wang, K.K. Fung, N. Wang, ZnO hierarchical structures for efficient quasi-solid dye-sensitized solar cells, Phys. Chem. Chem. Phys. 13 (2011) 10631–10634.
- [83] Y.J. Wang, Q.S. Wang, X. Zhan, F.M. Wang, M. Safdar, J. He, Visible light driven type II heterostructures and their enhanced photocatalysis properties: a review, Nanoscale 5 (2013) 8326–8339.
- [84] C.C. Nguyen, N.N. Vu, T.O. Do, Recent advances in the development of sunlight-driven hollow structure photocatalysts and their applications, J. Mater. Chem. A 36 (2015) 18345–18359.
- [85] A.J. Bard, R. Parsons, J. Jordan (Eds.), Standard Potentials in Aqueous Solution, Marcel Dekker, New York, 1985.
- [86] Q.J. Xiang, J.G. Yu, P.K. Wong, Quantitative characterization of hydroxyl radicals produced by various photocatalysts, J. Colloid. Interface Sci. 357 (2011) 163–167.